Myocardial Tissue Phase Mapping with Cine Phase-Contrast MR Imaging: Regional Wall Motion Analysis in Healthy Volunteers[1]

Steffen E. Petersen, MD, DPhil
Bernd A. Jung, PhD
Frank Wiesmann, MD
Joseph B. Selvanayagam, MBBS, FRACP, DPhil
Jane M. Francis, DCRR, DNM
Juergen Hennig, PhD
Stefan Neubauer, MD, FRCP
Matthew D. Robson, PhD

Purpose: To establish prospectively a database of normal three-dimensional systolic and diastolic endocardial and epicardial velocity values for all myocardial segments in healthy volunteers by using cine phase-contrast velocity magnetic resonance imaging, also called tissue phase mapping (TPM).

Materials and Methods: The study was approved by the institutional ethics committee and was conducted according to principles of the Declaration of Helsinki; each subject provided informed written consent. Ninety-six healthy volunteers (57 [59%] men, 39 [41%] women; mean age, 38 years ± 12 [standard deviation]) underwent cardiac phase-contrast imaging with a black blood segmented k-space gradient-echo sequence for the analysis of three-dimensional myocardial velocity with high spatial resolution at 1.5 T on basal, midventricular, and apical short-axis views. Eighteen consecutive volunteers were imaged twice to determine interstudy reproducibility, and intra- and interobserver variability values were analyzed. Systolic and diastolic velocity curves were analyzed for peak velocity and time to peak velocity in the radial, circumferential, and longitudinal directions, as well as for torsion rate and longitudinal strain rate. Mixed-effects models with a random intercept for volunteers were used to test differences among the three ventricular sections and the transmural, endocardial, and epicardial parameters.

Results: TPM enabled reproducible assessment of myocardial velocity with small intra- and interobserver variability values. Systolic peak radial velocity was lowest at the apical level ($P < .001$); diastolic peak radial velocity was similar at all three myocardial levels ($P = .73$). As viewed from the apex, a relative counterclockwise rotation during systole was followed by a relative clockwise rotation of the apex against the base. Diastolic and systolic peak longitudinal velocity values decreased from base to apex ($P < .001$). A gradient between endocardium and epicardium was observed for radial velocity values, with greater endocardial velocity values ($P < .001$).

Conclusion: TPM is a reproducible comprehensive modality for assessment of regional wall motion, and intra- and interobserver variability values are low.

[1] From the University of Oxford Centre for Clinical Magnetic Resonance Research (S.E.P., F.W., J.B.S., J.M.F., S.N., M.D.R.), Departments of Cardiovascular Medicine (S.E.P., F.W., J.B.S., J.M.F., S.N., M.D.R.) and Biochemistry (J.B.S.), University of Oxford, John Radcliffe Hospital, Oxford OX3 9DU, England; and Section of Medical Physics, Department of Radiology, University of Freiburg, Freiburg, Germany (B.A.J., J.H.). Received November 23, 2004; revision requested January 26, 2005; final revision received April 13; accepted March 16; final version accepted May 17. Supported by grants from the German Academic Exchange Service (S.E.P.), the British Heart Foundation (S.N.), and the Wellcome Trust (F.W., J.B.S.). **Address correspondence to** S.E.P. e-mail: *steffen.petersen@cardiov.ox.ac.uk*).

Assessment of myocardial regional wall motion plays a key role in many diagnostic and therapeutic decisions in current clinical practice. Studies about both stress-induced ischemia and about myocardial viability (ie, high- and low-dose dobutamine stress echocardiography [1], respectively) or about cardiovascular magnetic resonance (MR) imaging (2) are based on regional wall motion analysis results. Semiquantitative grading of regional wall motion is the most frequently applied technique, but it is highly subjective and has limited reproducibility. Despite dramatic improvements in echocardiography and cardiovascular MR imaging technology that permit quantitative and objective regional wall motion analysis, none of these has yet been widely applied in clinical practice. A possible explanation for this lack of application is that no existing technique has as yet provided noninvasive, quantitative, reproducible, three-dimensional systolic and diastolic regional wall motion analysis with sufficient spatial resolution to allow identification of transmural variation (endocardial and epicardial differences) in all myocardial segments (3).

Tissue Doppler ultrasonography (US), strain imaging, and strain-rate imaging with echocardiography are highly dependent on transducer angulation and thus have inherent limitations in regard to complete three-dimensional myocardial coverage and reproducibility (4,5). Cardiovascular MR imaging offers different techniques for regional wall motion analysis: myocardial tagging (6–13), phase velocity (11,14–20), phase displacement (21–23), and optical flow methods (24). Tagging approaches deliberately obliterate lines or grids of signal and watch-grid deformation, as these regions move during the cardiac cycle. Phase-velocity–based methods allow direct observation of the velocity of the tissue by using the phase of the signal, hence the term *tissue phase mapping* (TPM), and allow determination of the displacement with integration over time. Traditionally, TPM methods have been used to measure the displacement during short intervals and yield measurements of instantaneous velocity; the interval can be extended with use of the displacement encoding with stimulated echoes (or DENSE) approach (21–23) that allows measurement of displacement during most of the cardiac cycle. Optical flow of cine MR images provides an alternative approach for defining cardiac velocity values and displacement, and with it, high-resolution cine MR images that are not encoded with additional displacement information are used. Computerized algorithms are used to generate motion fields that explain the evolution of the images from one frame to the next. Such an approach is an extension of the function that is performed naturally by the human brain (24).

We hypothesized that TPM would allow quantitative measurements of motion parameters that are reproducible and independent of analyzers. Further, given the high spatial resolution of TPM, we hypothesized that this method would show differences between endocardium and epicardium for radial, circumferential, and longitudinal velocity parameters in healthy volunteers. Thus, the purpose of our study was to establish prospectively a database of normal three-dimensional systolic and diastolic endocardial and epicardial velocity values for all myocardial segments in healthy volunteers by using cine phase-contrast velocity MR imaging (also called TPM).

Materials and Methods

Study Participants

Ninety-six healthy volunteers (57 [59%] men, 39 [41%] women; mean age, 38 years ± 12 [standard deviation]) with normal electrocardiograms were enrolled to undergo cardiovascular MR imaging. The mean age of men (39 years ± 13) was similar to that of women (37 years ± 12) ($P > .05$). None of the subjects indicated that they had a history of cardiovascular disease, diabetes, cardiovascular symptoms, or long-term use of medication other than contraceptives. The study was performed according to the principles of the Declaration of Helsinki and was approved by the Oxfordshire Clinical Research Ethics Committee. Each subject provided informed written consent. Baseline characteristics of the healthy volunteers are included in Table 1.

MR Imaging

All cardiovascular MR imaging examinations were performed with a 1.5-T MR imager (Sonata; Siemens Medical Solutions, Erlangen, Germany). After piloting was performed, steady-state free precession cine images (repetition time msec/echo time msec, 3.0/1.5; flip angle, 60°; section thickness, 7 mm; intersection gap, 3 mm; temporal resolution, 45 msec; number of lines of k-space per heartbeat, 15; number of heartbeats per breath hold, 14–17) were acquired in horizontal and vertical long-axis views, and short-axis views were obtained parallel to the atrioventricular groove and included the entire left ventricle.

Phase-contrast images were acquired with a prospectively triggered black blood segmented k-space gradient-echo sequence (6.2/4.5; flip angle, 15°) with first-order flow compensation in all dimensions to minimize artifacts from flow or motion, and this technique is described in detail elsewhere (15,16). The pixel size was 2.7 × 1.3 mm (255 × 340-mm field of view, with 96 × 256 matrix interpolated to 192 × 256), and

Published online before print
10.1148/radiol.2383041992

Radiology 2006; 238:816–826

Abbreviations:
LV = left ventricular
TPM = tissue phase mapping

Author contributions:
Guarantors of integrity of entire study, S.E.P., S.N., M.D.R.; study concepts/study design or data acquisition or data analysis/interpretation, all authors; manuscript drafting or manuscript revision for important intellectual content, all authors; approval of final version of submitted manuscript, all authors; literature research, S.E.P., B.A.J., J.B.S., M.D.R.; clinical studies, S.E.P., B.A.J., F.W., J.B.S., J.M.F., J.H., M.D.R.; statistical analysis, S.E.P.; and manuscript editing, all authors

Authors stated no financial relationship to disclose.

the section thickness was 8 mm. Velocity encoding was performed by adding a bipolar gradient in the read, phase, and section directions to the otherwise identical sequence after each radiofrequency pulse (in-plane velocity encoding, 20 cm/sec; through-plane velocity encoding, 30 cm/sec). The temporal resolution was 37–87 msec in a single breath hold (baseline and x-, y- and z-axis velocity components) during 17–29 heartbeats (adjustable to breath-holding capability). The temporal resolution was achieved by using view-sharing techniques for which the resulting velocity errors have been shown to be small in structures that are the size of the myocardium (16). The temporal resolution (mean, 62 msec ± 12) used for our study population had very low correlation coefficients for midventricular radial peak systolic ($r = 0.003$) and diastolic ($r = 0.19$) velocity values, and these values suggested that the temporal resolution applied would not substantially confound the acquired velocity parameters.

Three short-axis sections at basal (between the LV outflow tract and the papillary muscles), midventricular, and apical levels were acquired according to recommended guidelines (3). The typical distance between the basal and the apical short-axis section was 4–6 cm, and positioning of the sections, which was expressed as the percentage of the distance between the atrioventricular groove and the apex in the horizontal long axis, showed low variability. The basal, midventricular, and apical sections were located at means of 28% ± 5, 51% ± 4, and 74% ± 5, respectively, of that distance. All acquired data sets were of sufficient image quality, without respiratory artifacts in the magnitude images, and could be included in the analysis (Fig 1).

The first consecutive 18 of 96 healthy volunteers were imaged twice within 1 week to determine interstudy reproducibility. The mean age of men ($n = 8$; 36 years ± 15) in this group was similar to that of women ($n = 10$; 37 years ± 14) ($P > .05$). These 18 repeat sets of TPM data were acquired with an initial sequence that provided only radial and circumferential velocity information. Consequently, no variability information was available for longitudinal velocity and strain rate.

Data Analysis

Cine images were analyzed manually by one author (S.E.P., with 6 years of experience in cardiac MR imaging) with

Table 1

Baseline Characteristics and LV Volume Results in 96 Healthy Volunteers

Data	Value*
Characteristic	
Age (y)	38 ± 12
No. of patients	
Men	57
Women	39
Height (cm)	174 ± 8
Weight (kg)	73.0 ± 12.9
Body surface area (m^2)	1.87 ± 0.19
Heart rate (beats/min)	65 ± 10
Duration of systole (msec)	324 ± 34
Systolic blood pressure (mm Hg)	123 ± 18
Diastolic blood pressure (mm Hg)	81 ± 17
LV volume parameter	
LV ejection fraction (%)†	69 ± 6
LV mass index (g/m^2)‡	58.7 ± 10.5
LV end-diastolic volume index (mL/m^2)§	80 ± 12
LV end-systolic volume index (mL/m^2)	25 ± 7
LV stroke volume index (mL/m^2)	55 ± 8

Note.—LV = left ventricular.

* Except where indicated otherwise, values are the mean ± standard deviation.

† The normal range for male patients is 55%–73%, and that for female patients is 54%–74%, according to Alfakih et al (25).

‡ The normal range for male patients is 46–83 g/m^2, and that for female patients is 37–67 g/m^2, according to Alfakih et al (25).

§ The normal range for male patients is 53–112 mL/m^2, and that for female patients is 56–99 mL/m^2, according to Alfakih et al (25).

Figure 1

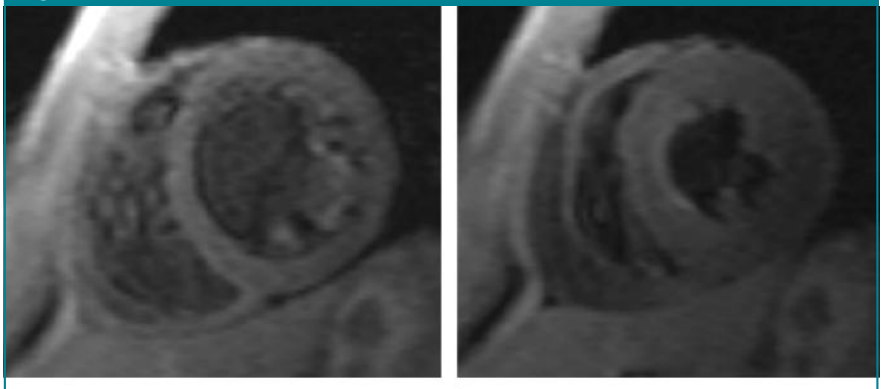

a. b.

Figure 1: **(a)** End-diastolic and **(b)** end-systolic magnitude images obtained at midventricular level by using a black blood segmented k-space gradient-echo sequence (also called TPM) in a healthy 31-year-old male volunteer.

software (Argus and Syngo 2002B; Siemens Medical Solutions), with exclusion of papillary muscles from the blood pool in end diastole and end systole. For each set of cine images, standard LV volume parameters were generated to further document healthiness of the volunteers (Table 1) as follows: LV ejection fraction, LV mass index, LV end-diastolic volume index, LV end-systolic volume index, and LV stroke volume index. All parameters were within normal limits. TPM data analysis was performed at a personal computer with customized software (Matlab, version 6.5; Mathworks, Natick, Mass) (17). After manual endocardial and epicardial contour segmentation performed by one author (S.E.P.) and a correction for translational motion components of the left ventricle in the image plane (15), radial and circumferential velocity values were calculated from in-plane velocities for each pixel on the basis of an internal polar coordinate system positioned at the center of mass of the left ventricle. The longitudinal velocity values were already encoded in the acquisition and were used without correction. The mean velocity was computed for pixels within the epicardial (inner half of the wall thickness), endocardial (outer half of the wall thickness), and transmural regions for each of the 16 segments of the 17-segment model according to the American Heart Association and American College of Cardiology recommendations (3).

The temporal axis of the three-dimensional systolic velocity information obtained was then normalized to the end-systolic time, as defined by the smallest LV cavity on midventricular cine images to avoid temporal jitter. Diastolic velocity information was similarly normalized to the duration of diastole (duration of systole subtracted from R-R interval). For each of the radial and longitudinal velocity values, two systolic and two diastolic parameters were computed: systolic peak velocity, systolic time to peak velocity, diastolic peak velocity, and diastolic time to peak velocity. These parameters were computed for endocardial, epicardial, and transmural velocity values in 16 segments (3) and for averaged global basal, midventricular, and apical velocity values.

In addition, the relative speed of motion between the basal and apical sections was plotted during the cardiac cycle as the difference between the circumferential (torsion rate [degree · sec^{-1} · cm^{-1}], defined as the rate of change of angular velocity along the heart) and the longitudinal (longitudinal strain rate [sec^{-1}]) velocity values of the global basal and apical sections normalized to the midventricular short-axis diameter and to the ventricular length. Peak systolic torsion rate, peak diastolic torsion rate, systolic time to peak torsion rate, diastolic time to peak torsion rate, peak systolic longitudinal strain rate, peak diastolic longitudinal strain rate, systolic time to peak systolic longitudinal strain rate, and diastolic time to peak longitudinal strain rate were then derived from those graphs.

One observer (S.E.P.) analyzed the images in the first 18 volunteers twice, with 6 months between analyses, and these data were also analyzed by a second observer (F.W., with 8 years of experience in cardiac MR imaging) to allow determination of intra- and interobserver variability, respectively.

Statistical Analysis

All data are presented as the mean ± standard deviation unless stated other-

Figure 2

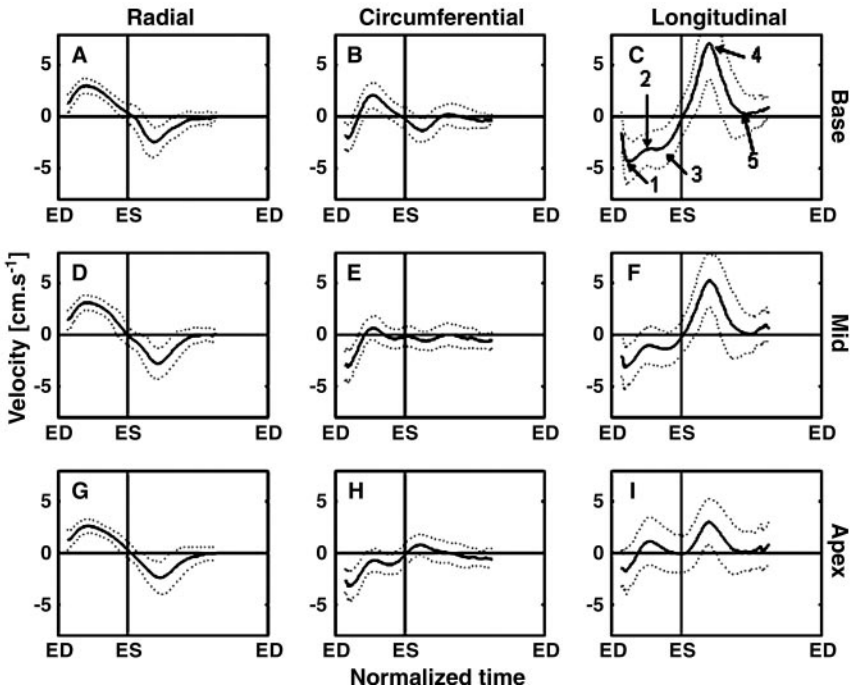

Figure 2: Graphs show data from three-dimensional TPM of basal (top row), midventricular (middle row), and apical (bottom row) short-axis views. Data are presented as mean (solid line) ± standard deviation (dashed lines) after piecewise cubic Hermite interpolation. *A*, *D*, and *G* show radial velocity ($n = 96$) information; positive velocity values represent contraction and negative velocity values represent expansion. *B*, *E*, and *H* display circumferential velocity values ($n = 96$); positive velocity values represent clockwise rotation and negative velocity values represent counterclockwise rotation. *C*, *F*, and *I* show plots for longitudinal velocity values ($n = 78$); positive velocity values indicate base movement away from the apex, and negative velocity values indicate base movement toward the apex. Longitudinal velocity values during the cardiac cycle can be classified into five steps: The base of the heart undergoes initial displacement toward the apex (step *1*) followed by a decrease in velocity (step *2*). At end systole *(ES)*, a small increase in velocity directed toward the apex occurs (step *3*) before rapid motion of the base away from the apex during early diastole (step *4*). This is followed by a rapid decrease in velocity (step *5*). *ED* = end diastole, *Mid* = midventricle.

wise. To establish differences in continuous data among data obtained for the base, the midventricle, and the apex and to compare endocardial and epicardial parameters (transmural gradient), mixed-effects models were fitted (Stata 8.0; StataCorp, College Station, Tex), with a random intercept for volunteer and categoric fixed effects for sector and transmural gradient. Throughout the analyses, a two-tailed *P* value of less than .05 was considered to indicate a statistically significant difference.

For analysis of interstudy reproducibility and inter- and intraobserver variability, the mean difference ± the standard deviation of the mean difference were determined (26). All other computations were performed with software (SPSS 11.5, SPSS, Chicago, Ill; Matlab, version 6.5, Mathworks).

Results

Radial Velocity

Contraction (positive radial velocity values) and expansion (relaxation, negative radial velocity values) patterns in the basal, midventricular, and apical levels were characterized by an increase in contraction velocity during early systole, followed by a slowing down of contraction velocity later in systole. The inverse pattern was observed in diastole. Similarly, an initial increase in radial expansion velocity values was followed by a decrease later during diastole (Fig 2).

Systolic peak radial velocity was lowest in the apex with the mixed-effects model ($z = -10.38$, $P < .001$), but the systolic time to peak radial velocity was similar at all levels ($z = -1.21$, $P = .23$) (Tables 2 and 3, Fig 3). The diastolic time to peak radial velocity was shorter in the basal section compared with that in the midventricular and in the apical sections ($z = 8.44$, $P < .001$), and these values were accompanied by similar diastolic peak radial velocity values at those myocardial levels ($z = 0.35$, $P = .73$).

Transmural gradients for systolic and diastolic peak radial velocity values could be observed in each myocardial section ($P < .001$ across levels for both

Table 2

Segmental and Myocardial Layer Distribution of Systolic Radial and Longitudinal Velocity Parameters

Myocardial Layer	Basal Level	Midventricular Level	Apical Level
	Peak Radial Velocity (cm/sec)		
Epicardial	2.97 ± 1.22	3.09 ± 1.27	2.57 ± 0.96
Endocardial	3.92 ± 1.26	3.83 ± 1.12	3.22 ± 0.94
Transmural	3.44 ± 1.33	3.46 ± 1.25	2.90 ± 1.00
	Time to Peak Radial Velocity*		
Epicardial	47.8 ± 29.9	48.0 ± 25.3	46.0 ± 20.8
Endocardial	48.3 ± 25.6	47.4 ± 18.5	47.4 ± 16.1
Transmural	48.1 ± 27.8	47.7 ± 22.1	46.7 ± 18.6
	Peak Longitudinal Velocity (cm/sec)		
Epicardial	−5.59 ± 2.73	−4.14 ± 3.01	−2.66 ± 2.71
Endocardial	−5.65 ± 2.61	−4.11 ± 2.82	−2.71 ± 2.65
Transmural	−5.62 ± 2.67	−4.12 ± 2.92	−2.68 ± 2.68
	Time to Peak Longitudinal Velocity*		
Epicardial	37.3 ± 38.8	50.6 ± 61.0	64.4 ± 67.4
Endocardial	38.4 ± 41.8	54.4 ± 62.8	65.5 ± 67.2
Transmural	37.9 ± 40.3	52.5 ± 61.9	65.0 ± 67.3

Note.—Values are the mean ± standard deviation.

* Values are the percentage of end systole.

Table 3

Segmental and Myocardial Layer Distribution of Diastolic Radial and Longitudinal Velocity Parameters

Myocardial Layer	Basal Level	Midventricular Level	Apical Level
	Peak Radial Velocity (cm/sec)		
Epicardial	−3.52 ± 1.71	−3.72 ± 1.54	−3.36 ± 1.37
Endocardial	−4.62 ± 2.13	−5.05 ± 1.80	−4.61 ± 1.56
Transmural	−4.07 ± 2.01	−4.38 ± 1.80	−3.98 ± 1.60
	Time to Peak Radial Velocity*		
Epicardial	21.7 ± 11.2	23.1 ± 11.1	26.0 ± 11.5
Endocardial	21.5 ± 10.5	21.4 ± 11.7	25.6 ± 9.56
Transmural	21.6 ± 10.8	22.2 ± 11.4	25.8 ± 10.6
	Peak Longitudinal Velocity (cm/sec)		
Epicardial	9.25 ± 3.04	6.94 ± 2.80	4.27 ± 2.49
Endocardial	9.59 ± 3.18	7.28 ± 2.80	4.35 ± 2.45
Transmural	9.42 ± 3.11	7.11 ± 2.80	4.31 ± 2.47
	Time to Peak Longitudinal Velocity*		
Epicardial	21.7 ± 7.36	22.7 ± 8.19	15.2 ± 17.7
Endocardial	21.5 ± 7.54	22.2 ± 8.90	11.7 ± 19.4
Transmural	21.6 ± 7.45	22.4 ± 8.55	13.4 ± 18.7

Note.—Values are the mean ± standard deviation.

* Values are the percentage of end diastole.

systolic and diastolic velocities), with higher endocardial than epicardial velocity values (Fig 3).

Circumferential Velocity and Torsion Rate

During systole, a counterclockwise rotation (negative velocity values in Fig 2), as viewed from the apex, was followed by a clockwise rotation (positive velocity values in Fig 2) in the base and at the midventricular level. The apical myocardium, however, showed a counterclockwise rotation during the entire length of systole. Circumferential velocity values were generally lower during diastole. The base revealed a counterclockwise rotation in contrast to a clockwise rotation in the apex during diastole. Consequently, peak velocity values and time-to-peak value parameters for clockwise and counterclockwise rotations were systolic or diastolic, depending on the location of the myocardial segments. Therefore, we plotted the torsion rate during the cardiac cycle (Fig 4a). A relative counterclockwise rotation during systole was followed by a relative clockwise rotation of the apex against the base. Peak systolic torsion rate, peak diastolic torsion rate, time to peak systolic torsion rate, and time to peak diastolic torsion rate are shown in Table 4.

Figure 3

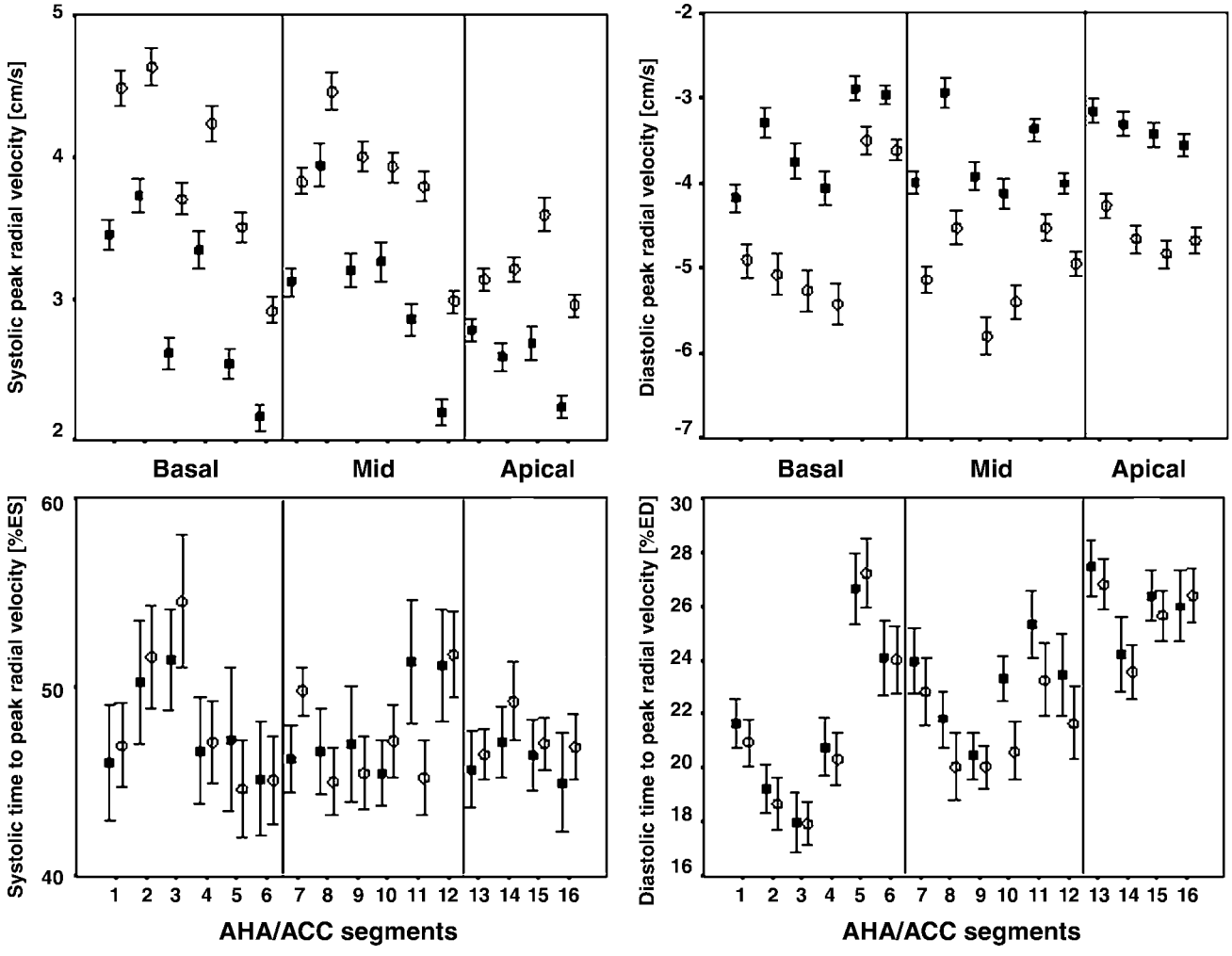

Figure 3: Graphs show segmental and myocardial layer distribution of radial velocity parameters ($n = 96$). Segments *1–6* are basal, *7–12* are midventricular, and *13–16* are apical, according to American Heart Association *(AHA)* and American College of Cardiology *(ACC)* recommendations (3). Epicardial (■) and endocardial (○) velocity parameters are shown as mean ± standard error of the mean. Positive radial velocity values indicate contraction; and negative radial velocity values, expansion. Transmural gradients for systolic and diastolic peak radial velocity values are observed in each of the three myocardial levels ($P < .001$ for both), with higher absolute endocardial velocity values than epicardial velocity values. The basal, midventricular *(Mid),* and apical sections were located at points that signify the percentage of the distance between the atrioventricular groove and the apex in the horizontal long axis of 28% ± 5, 51% ± 4, and 74% ± 5, respectively. The error bars signify ± 1 standard error of the mean. *ED* = end diastole, *ES* = end systole.

Figure 4

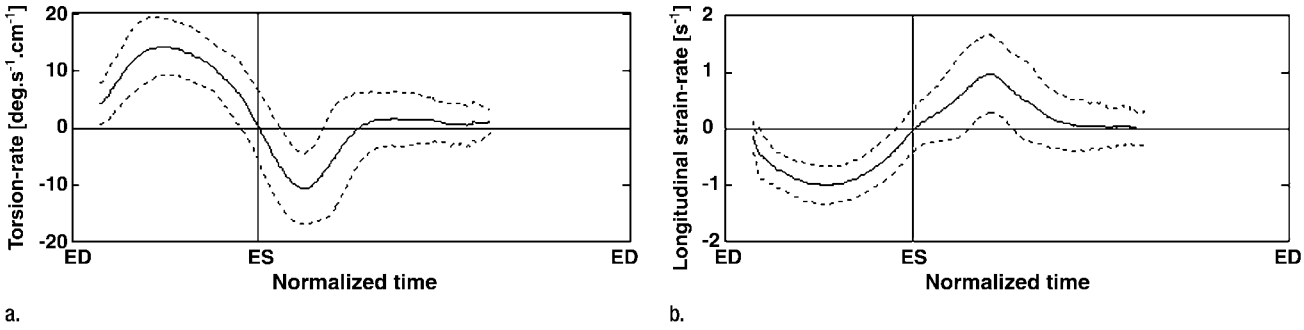

Figure 4: Graphs show **(a)** myocardial torsion rate ($n = 96$) and **(b)** myocardial longitudinal strain rate ($n = 78$). Data in graphs are presented as mean (solid line) ± 1 standard deviation (dashed lines) after piecewise cubic Hermite interpolation. Relative counterclockwise rotation during systole is followed by a relative clockwise rotation of the apex against the base. On **b**, basal movement occurs toward the apex during systole and away from the apex during diastole. *ED* = end diastole, *ES* = end systole.

No statistically significant differences between endocardial and epicardial velocity values were observed for clockwise and counterclockwise peak velocity values and time to peak circumferential velocity values ($P > .05$ for all).

Longitudinal Velocity and Longitudinal Strain Rate

Longitudinal velocity values during the cardiac cycle could be classified into five steps (the numbers of the steps correspond to those in Fig 2): The base of the heart underwent an initial displacement toward the apex (step 1 [mean peak systolic longitudinal velocity of −5.3 cm/sec ± 2.0]), followed by a decrease in velocity (step 2). At end systole, a small increase in velocity directed toward the apex occurred (step 3) before rapid motion of the base away from the apex during early diastole (step 4 [mean peak diastolic longitudinal velocity of 9.2 cm/sec ± 2.5]). This was followed by a rapid decrease in velocity away from the apex (step 5). The same pattern of motion was present at the midventricular (mean peak systolic and diastolic longitudinal velocity values of −3.7 cm/sec ± 2.1 and 7.0 cm/sec ± 2.3, respectively) and apical (mean peak systolic and diastolic longitudinal velocity values of −2.2 cm/sec ± 2.1 and 4.1 cm/sec ± 2.0, respectively) levels, with decreasing amplitudes. Maximal basal movement toward the apex occurred during systole and away from the apex during diastole (Fig 4b).

Table 4

Myocardial Torsion and Longitudinal Strain Rates in Healthy Volunteers

Parameter	Value*
Peak systolic torsion rate ($n = 96$)†	16.2 ± 4.7
Time to peak systolic torsion rate ($n = 96$)‡	53 ± 21
Peak diastolic torsion rate ($n = 96$)†	−15.0 ± 5.7
Time to peak diastolic torsion rate ($n = 96$)§	13 ± 8
Peak systolic longitudinal strain rate ($n = 78$)‖	−1.09 ± 0.32
Time to peak systolic longitudinal strain rate ($n = 78$)‡	51 ± 13
Peak diastolic longitudinal strain rate ($n = 78$)‖	1.49 ± 0.60
Time to peak diastolic longitudinal strain rate ($n = 78$)§	23 ± 8

* Values are the mean ± standard deviation.

† Values are degree · sec^{-1} · cm^{-1}.

‡ Values are percentage of end systole (ie, quotient of time from R wave divided by time from R wave to end systole).

§ Values are percentage of end diastole (ie, quotient of time from end systole divided by time from end systole to R wave).

‖ Values are sec^{-1}.

Systolic peak ($z = -0.25$, $P = .81$) and time to peak ($z = 1.04$, $P = .30$) longitudinal velocity values were similar in the endocardial and epicardial layers, while diastolic peak ($z = 3.12$, $P = .002$) and time to peak ($z = -2.72$, $P = .006$) longitudinal velocity values differed. Both diastolic ($z = -44.64$, $P < .001$) and systolic ($z = 27.11$, $P < .001$) peak longitudinal velocity values decreased from base to apex (Tables 2 and 3, Fig 5).

Intra- and Interobserver Variability and Interstudy Reproducibility

Intra- and interobserver variability were low and interstudy reproducibility was high for all velocity parameters at apical, midventricular, and basal levels (Table 5, Fig 6).

Discussion

Both of the mature cardiovascular MR imaging–based methods, tagging and TPM, essentially are used to evaluate myocardial motion. TPM offers the better spatial resolution, whereas tagging has a better temporal resolution and may thus be superior in terms of identification of peak deformation. TPM covers most of the cardiac cycle and allows quantification of endocardial and epicardial wall motion in both systole and a large portion of diastole with consistent data quality, whereas tag fading pre-

vented diastolic motion assessment until newer tagging sequences were introduced. TPM data acquisition and postprocessing are quick and simple in contrast to the time-consuming and complex tagging analysis, although the latter is continually being improved (27,28). The temporal resolution for TPM could potentially be improved with use of a navigator sequence, although such an approach would remove the need for breath holding but might increase the total imaging time. Within the temporal resolution applied in our study population, no dependency was found for peak systolic and diastolic midventricular radial velocity. This lack of dependency suggests that the current range of temporal resolution for TPM might be sufficient.

Typical transmural radial velocity patterns in healthy hearts have been described by Markl and co-workers (17) by using TPM and agree with our findings. In addition, we report transmural differences with higher systolic and diastolic endocardial than epicardial radial velocity values. Hashimoto and colleagues (29) found an increase in systolic and diastolic strain rate in sections from the endocardium to the midmyocardium to the epicardium in an animal model, but they did not observe significant differences in myocardial velocity values by using tissue Doppler US. This discrepancy might be partly explained

Figure 5

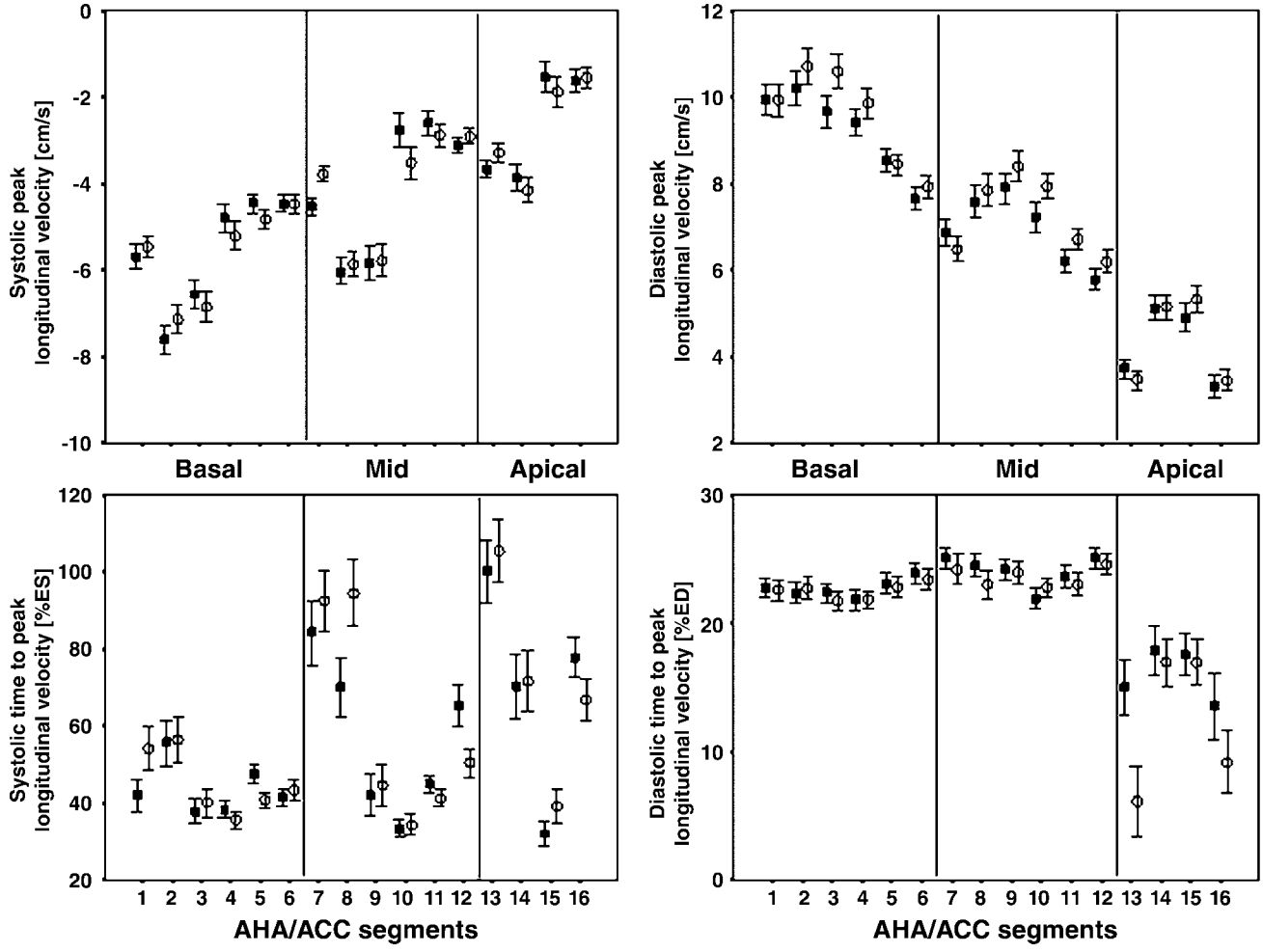

Figure 5: Graphs show segmental and myocardial layer distribution of longitudinal velocity parameters ($n = 78$). Segments *1–6* are basal, *7–12* are midventricular, and *13–16* are apical, according to American Heart Association *(AHA)* and American College of Cardiology *(ACC)* recommendations (3). Epicardial (■) and endocardial (○) velocity parameters are shown as mean ± standard error of the mean. Positive longitudinal velocity values indicate base movement away from the apex; and negative values, base movement toward the apex. Systolic peak ($z = -0.25$, $P = .81$) and time to peak ($z = 1.04$, $P = .30$) longitudinal velocity values were similar in the endocardial and epicardial layers, whereas diastolic peak ($z = 3.12$, $P = .002$) and time to peak ($z = -2.72$, $P = .006$) longitudinal velocity values differed. Both diastolic ($z = -44.64$, $P < .001$) and systolic ($z = 27.11$, $P < .001$) peak longitudinal velocity values decreased from base to apex. The error bars signify ± 1 standard error of the mean. *ED* = end diastole, *ES* = end systole.

Table 5

Intra- and Interobserver Variability and Interstudy Reproducibility at Basal, Midventricular, and Apical Level

Parameter and Level	Value for 18 Healthy Volunteers*	Intraobserver Variability†	Interobserver Variability†	Interstudy Reproducibility†
Systolic peak radial velocity‡				
Basal	2.70 ± 0.63	−0.009 ± 0.17	0.02 ± 0.13	−0.003 ± 0.59
Midventricular	2.94 ± 0.71	−0.07 ± 0.29	0.005 ± 0.31	−0.12 ± 0.84
Apical	2.40 ± 0.75	−0.04 ± 0.13	0.02 ± 0.13	0.18 ± 0.76
Diastolic peak radial velocity‡				
Basal	−3.05 ± 1.06	−0.04 ± 0.37	−0.05 ± 0.36	−0.72 ± 1.46
Midventricular	−3.88 ± 1.33	−0.10 ± 0.25	−0.06 ± 0.21	−0.76 ± 1.84
Apical	−4.03 ± 1.33	−0.08 ± 0.17	0.04 ± 0.13	−0.37 ± 1.55
Clockwise peak circumferential velocity‡				
Basal	2.48 ± 0.55	−0.16 ± 0.34	0.04 ± 0.11	0.51 ± 1.03
Midventricular	1.61 ± 0.69	−0.04 ± 0.41	−0.05 ± 0.23	0.29 ± 0.87
Apical	1.80 ± 0.66	0.02 ± 0.11	0.05 ± 0.13	0.14 ± 0.87
Counterclockwise peak circumferential velocity‡				
Basal	−2.55 ± 1.03	−0.14 ± 0.65	−0.006 ± 0.10	−0.22 ± 1.43
Midventricular	−2.99 ± 1.37	0.02 ± 0.49	−0.03 ± 0.24	−0.72 ± 1.18
Apical	−2.97 ± 1.31	−0.03 ± 0.09	0.04 ± 0.12	−0.56 ± 1.12
Peak systolic torsion rate§	12.6 ± 4.6	0.3 ± 1.1	0.2 ± 0.6	0.1 ± 5.7
Peak diastolic torsion rate§	−14.3 ± 5.7	0.2 ± 1.1	−0.1 ± 0.6	−3.4 ± 7.4

* Values are the mean ± 1 standard deviation.

† Values are the mean difference ± standard deviation.

‡ Values are centimeters per second.

§ Values are degree · sec^{-1} · cm^{-1}. Because the torsion rate is defined as the rate of change of angular velocity along the heart and is calculated as the difference between circumferential velocity values of the global basal and apical sections normalized to the midventricular short-axis diameter, there are no values for the three myocardial levels.

Figure 6

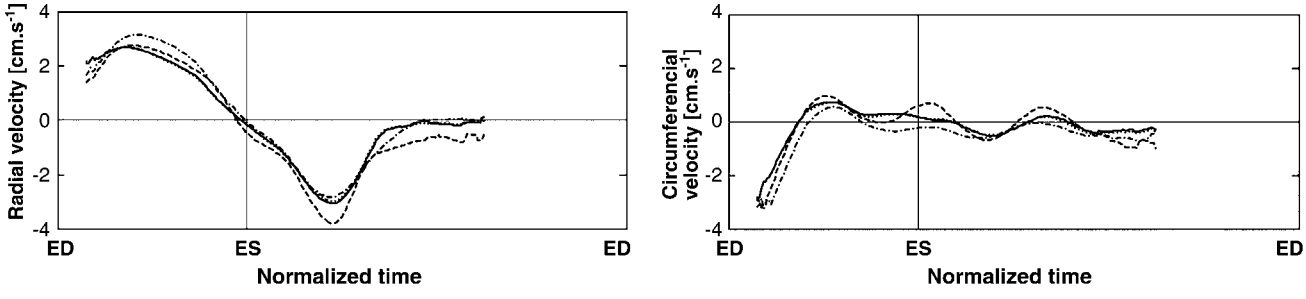

a. b.

Figure 6: Graphs show intra- and interobserver variability and interstudy reproducibility for **(a)** radial and **(b)** circumferential velocity values during the cardiac cycle at midventricular level as the mean value for the first 18 consecutive healthy volunteers. Data for observer 1 and measurement 1 (solid line), for observer 1 and measurement 2 (dashed-dotted line), and for observer 2 (dashed line) and second image (dotted line) were plotted. Note the small variation in systolic and diastolic peak velocity values and systolic and diastolic time to peak velocity values. Keys are the same as those for Figure 4.

by the slightly better spatial resolution for TPM (2.7 × 1.3 mm for TPM vs <3 × <2 mm for tissue Doppler US imaging [28]) and more likely by the fact that, in our study, we compared only two rather than three myocardial layer velocity values. The lower systolic peak radial velocity values at the apex might reflect the fact that this region is constrained by the diaphragm. Smaller diastolic peak radial velocity values in the basal myocardium compared with those in the midventricular and apical myocardium might be explained by the proportionally smaller myocardium-to-cavity area at the base of the heart.

Our findings of a counterclockwise rotation followed by a clockwise rotation in the base of the heart during systole and the apical counterclockwise rotation during the entire length of sys-

tole, as viewed from the apex, are consistent with findings in studies with cardiovascular MR tagging (30). This pattern of circumferential velocity in the myocardium is responsible for the fact that peak circumferential clockwise and counterclockwise velocity values occur quite variably during either systole or diastole. Plotting the torsion rate as the difference between the basal and apical circumferential velocity values by normalizing the velocity values according to the distance between these sections, we obtained the basic system-independent measurement of this motion. This allows determination of true systolic and diastolic parameters, such as peak systolic torsion rate, time to peak systolic torsion rate, peak diastolic torsion rate, and time to peak diastolic torsion rate. We did not find a transmural gradient of circumferential velocity values, a finding that is consistent with three-dimensional tagging results reported by Moore and colleagues (30).

Our results for mean diastolic peak longitudinal velocity at the myocardial base (9.2 cm/sec ± 2.5) match those for basal mean longitudinal velocity values with the use of TPM (8.2 cm/sec ± 2.2) reported by Karwatowski et al (31). Similarly, the decrease in longitudinal velocity values from base to apex observed in our cohort was confirmed by findings in a previous study on echocardiography, with mean peak systolic and diastolic longitudinal velocity values at the basal level of −9.3 cm/sec ± 1.3 and 14.8 cm/sec ± 3.2, respectively, and those at the midventricular level of −7.7 cm/sec ± 1.6 and 12.3 cm/sec ± 2.8, respectively (32). Longitudinal velocity values were generally smaller with use of TPM compared with those with use of echocardiography, and this finding might be explained by the better temporal resolution at echocardiography than at TPM. Surprisingly, we could not detect a statistically significant transmural gradient for peak systolic longitudinal velocity values, although longitudinally directed fibers are mainly located in the subendocardium (33,34). A possible explanation might lie in the helical orientation of the epicardial fibers (35), an orientation that potentially only inhibits systolic transmural velocity differences, as peak diastolic longitudinal velocity values were greater in the endocardial layers.

Our results suggest that TPM is a reproducible comprehensive modality for assessment of regional wall motion, and intra- and interobserver variability values are low. For analyses of longitudinal velocity values, findings in a previous study (30) suggested that reproducibility is high in the assessment of patients twice but within the same imaging time. The variation seen in true interstudy reproducibility, however, should reflect not only variability in measurement but also varying preload, blood pressure, and different section selection, and this variability of all these factors necessitates the acquisition of images at separate times. The variability in section positioning in our study population was very low (≤5%, calculated by dividing the standard deviation by the mean of the position of the section; the position of the section was expressed as a percentage of the distance of the section to the mitral valve plane divided by the distance between the mitral valve plane and the apex). Interobserver variability found in our study compares favorably with that obtained for echocardiographic strain and strain-rate imaging (approximately 15%) (36).

Our study was performed in young healthy volunteers and was not designed for investigation of effects of age, preload, and medication on myocardial velocity values. The effects on the described parameters will have to be addressed in future studies.

TPM currently is limited because of a lower temporal resolution when compared with echocardiographically determined strain and strain rate (5) (one order of magnitude) and cardiovascular MR tagging (30) (two- to threefold). Furthermore, the prospectively electrocardiographically triggered TPM naturally misses about 10%–20% of the cardiac cycle in late diastole. High-field-strength magnets, improved gradient systems, and implementation of parallel imaging may further improve temporal resolution.

An inherent problem in the use of myocardial velocity parameters is caused by the nature of continuous structures, such as the myocardium, to transmit deformation to adjacent tissue, and the transmittal of deformation often is referred to as "tethering." Any locally measured myocardial velocity might reflect active or passive motion (37–39). As described in detail elsewhere (15), TPM is performed in a breath hold to avoid bulk motion of the internal organs, and it corrects in-plane translational motion. Furthermore, our measurements of torsion rate and longitudinal strain rate are independent of tethering effects.

In conclusion, TPM is a reproducible comprehensive modality for assessment of regional wall motion, and intra- and interobserver variability values are low. Our results may potentially serve as reference data with which data from abnormal hearts can be compared, allowing TPM to be used as part of a multiparametric cardiovascular MR imaging approach in clinical practice.

Acknowledgments: We thank Christine H. Lorenz, PhD, for invaluable discussions, Lucy E. Hudsmith, MA, MRCP, for help in data acquisition, and Helen Doll, DPhil, for excellent statistical support.

References

1. Mazur W, Nagueh SF. Myocardial viability: recent developments in detection and clinical significance. Curr Opin Cardiol 2001;16:277–281.

2. Nagel E, Lehmkuhl HB, Bocksch W, et al. Noninvasive diagnosis of ischemia-induced wall motion abnormalities with the use of high-dose dobutamine stress MRI: comparison with dobutamine stress echocardiography. Circulation 1999;99:763–770.

3. Cerqueira MD, Weissman NJ, Dilsizian V, et al. Standardized myocardial segmentation and nomenclature for tomographic imaging of the heart: a statement for healthcare professionals from the Cardiac Imaging Committee of the Council on Clinical Cardiology of the American Heart Association. Circulation 2002;105:539–542.

4. Voigt JU, Flachskampf FA. Strain and strain rate: new and clinically relevant echo parameters of regional myocardial function. Z Kardiol 2004;93:249–258.

5. Pellerin D, Sharma R, Elliott P, Veyrat C. Tissue Doppler, strain, and strain rate echo-

cardiography for the assessment of left and right systolic ventricular function. Heart 2003;89(suppl 3): iii9–iii17.

6. Young AA, Kramer CM, Ferrari VA, Axel L, Reichek N. Three-dimensional left ventricular deformation in hypertrophic cardiomyopathy. Circulation 1994;90:854–867.
7. Reichek N. MRI myocardial tagging. J Magn Reson Imaging 1999;10:609–616.
8. Maier SE, Fischer SE, McKinnon GC, Hess OM, Krayenbuehl HP, Boesiger P. Evaluation of left ventricular segmental wall motion in hypertrophic cardiomyopathy with myocardial tagging. Circulation 1992;86:1919–1928.
9. Young AA, Imai H, Chang CN, Axel L. Two-dimensional left ventricular deformation during systole using magnetic resonance imaging with spatial modulation of magnetization. Circulation 1994;89:740–752.
10. Zerhouni EA, Parish DM, Rogers WJ, Yang A, Shapiro EP. Human heart: tagging with MR imaging—a method for noninvasive assessment of myocardial motion. Radiology 1988;169:59–63.
11. Henson RE, Song SK, Pastorek JS, Ackerman JJ, Lorenz CH. Left ventricular torsion is equal in mice and humans. Am J Physiol Heart Circ Physiol 2000;278:H1117–H1123.
12. McVeigh ER, Atalar E. Cardiac tagging with breath-hold cine MRI. Magn Reson Med 1992;28:318–327.
13. Rademakers FE, Rogers WJ, Guier WH, et al. Relation of regional cross-fiber shortening to wall thickening in the intact heart: three-dimensional strain analysis by NMR tagging. Circulation 1994;89:1174–1182.
14. Hennig J, Markl M, Schneider B, Peschl S. Regional myocardial function with tissue phase mapping. MAGMA 1998;6:145–146.
15. Hennig J, Schneider B, Peschl S, Markl M, Krause T, Laubenberger J. Analysis of myocardial motion based on velocity measurements with a black blood prepared segmented gradient-echo sequence: methodology and applications to normal volunteers and patients. J Magn Reson Imaging 1998;8:868–877.
16. Markl M, Hennig J. Phase contrast MRI with improved temporal resolution by view sharing: k-space related velocity mapping properties. Magn Reson Imaging 2001;19:669–676.
17. Markl M, Schneider B, Hennig J. Fast phase contrast cardiac magnetic resonance imaging: improved assessment and analysis of left ventricular wall motion. J Magn Reson Imaging 2002;15:642–653.
18. Markl M, Schneider B, Hennig J, et al. Cardiac phase contrast gradient echo MRI: measurement of myocardial wall motion in healthy volunteers and patients. Int J Card Imaging 1999;15:441–452.
19. Karwatowski SP, Mohiaddin R, Yang GZ, et al. Assessment of regional left ventricular long-axis motion with MR velocity mapping in healthy subjects. J Magn Reson Imaging 1994;4:151–155.
20. Pelc LR, Sayre J, Yun K, et al. Evaluation of myocardial motion tracking with cine-phase contrast magnetic resonance imaging. Invest Radiol 1994;29:1038–1042.
21. Kim D, Gilson WD, Kramer CM, Epstein FH. Myocardial tissue tracking with two-dimensional cine displacement-encoded MR imaging: development and initial evaluation. Radiology 2004;230:862–871.
22. Aletras AH, Balaban RS, Wen H. High-resolution strain analysis of the human heart with fast-DENSE. J Magn Reson 1999;140:41–57.
23. Aletras AH, Ding S, Balaban RS, Wen H. DENSE: displacement encoding with stimulated echoes in cardiac functional MRI. J Magn Reson 1999;137:247–252.
24. Amartur SC, Vesselle HJ. A new approach to study cardiac motion: the optical flow of cine MR images. Magn Reson Med 1993;29:59–67.
25. Alfakih K, Plein S, Thiele H, Jones T, Ridgway JP, Sivananthan MU. Normal human left and right ventricular dimensions for MRI as assessed by turbo gradient echo and steady-state free precession imaging sequences. J Magn Reson Imaging 2003;17:323–329.
26. Bland JM, Altman DG. Statistical methods for assessing agreement between two methods of clinical measurement. Lancet 1986;1:307–310.
27. Garot J, Bluemke DA, Osman NF, et al. Fast determination of regional myocardial strain fields from tagged cardiac images using harmonic phase MRI. Circulation 2000;101:981–988.
28. Osman NF, Kerwin WS, McVeigh ER, Prince JL. Cardiac motion tracking using CINE harmonic phase (HARP) magnetic resonance imaging. Magn Reson Med 1999;42:1048–1060.
29. Hashimoto I, Li X, Hejmadi Bhat A, Jones M, Zetts AD, Sahn DJ. Myocardial strain rate is a superior method for evaluation of left ventricular subendocardial function compared with tissue Doppler imaging. J Am Coll Cardiol 2003;42:1574–1583.
30. Moore CC, Lugo-Olivieri CH, McVeigh ER, Zerhouni EA. Three-dimensional systolic strain patterns in the normal human left ventricle: characterization with tagged MR imaging. Radiology 2000;214:453–466.
31. Karwatowski SP, Mohiaddin RH, Yang GZ, Firmin DN, St John Sutton M, Underwood SR. Regional myocardial velocity imaged by magnetic resonance in patients with ischaemic heart disease. Br Heart J 1994;72:332–338.
32. Galiuto L, Ignone G, DeMaria AN. Contraction and relaxation velocities of the normal left ventricle using pulsed-wave tissue Doppler echocardiography. Am J Cardiol 1998;81:609–614.
33. Simpson IA. Echocardiographic assessment of long axis function: a simple solution to a complex problem? Heart 1997;78:211–212.
34. Rushmer RF, Crystal DK, Wagner C. The functional anatomy of ventricular contraction. Circ Res 1953;1:162–170.
35. Torrent-Guasp FF, Whimster WF, Redmann K. A silicone rubber mould of the heart. Technol Health Care 1997;5:13–20.
36. Voigt JU, Arnold MF, Karlsson M, et al. Assessment of regional longitudinal myocardial strain rate derived from Doppler myocardial imaging indexes in normal and infarcted myocardium. J Am Soc Echocardiogr 2000;13:588–598.
37. Abraham TP, Belohlavek M, Thomson HL, et al. Time to onset of regional relaxation: feasibility, variability and utility of a novel index of regional myocardial function by strain rate imaging. J Am Coll Cardiol 2002;39:1531–1537.
38. Kukulski T, Jamal F, D'Hooge J, Bijnens B, De Scheerder I, Sutherland GR. Acute changes in systolic and diastolic events during clinical coronary angioplasty: a comparison of regional velocity, strain rate, and strain measurement. J Am Soc Echocardiogr 2002;15:1–12.
39. Urheim S, Edvardsen T, Torp H, Angelsen B, Smiseth OA. Myocardial strain by Doppler echocardiography: validation of a new method to quantify regional myocardial function. Circulation 2000;102:1158–1164.